

pubs.acs.org/JPCL Letter

# Observation of Core Phonon in Electron—Phonon Coupling in Au<sub>25</sub> Nanoclusters

Zhongyu Liu, Yingwei Li, Wonyong Shin, and Rongchao Jin\*



Cite This: J. Phys. Chem. Lett. 2021, 12, 1690–1695



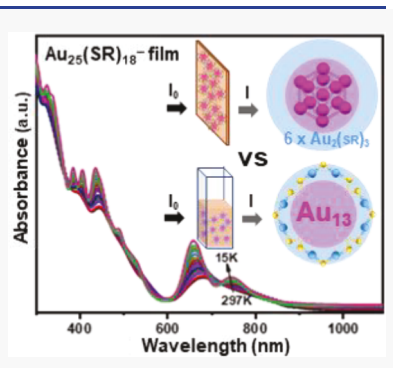
**ACCESS** 

Metrics & More



Supporting Information

**ABSTRACT:** Temperature-dependent optical properties are of paramount importance for fundamentally understanding the electron—phonon interactions and phonon modes in atomically precise nanocluster materials. In this work, low-temperature optical absorption spectra of the icosahedral  $[Au_{25}(SR)_{18}]^-$  nanocluster are measured from room temperature down to liquid helium temperature by adopting a thin-film-based technique. The thin-film measurement is further compared with results from the previous solution-based method. Interestingly, the previously missing core phonon is revealed by a quantitative analysis of the film data through peak deconvolution and fitting of the temperature trend with a theoretical model. The two lowest-energy absorption peaks (at 1.6 and 1.8 eV) of  $Au_{25}$  are determined to couple with the staple-shell phonon (average energy  $\sim 350 \text{ cm}^{-1}$ ) in the solution state, but in the solid state these electronic transitions couple with the core phonon (average energy  $\sim 180 \text{ cm}^{-1}$ ). The suppression of the staple-shell phonon in the solid state is attributed to the intracluster and cluster—matrix interactions.



A tomically precise Au nanoclusters (NCs), consisting of tens to hundreds of Au atoms per cluster with precise structures, offer many opportunities for tackling some fundamental issues in nanoscience research. Among the physicochemical properties, understanding the optical properties and carrier dynamics of metal NCs is of paramount importance to their applications (such as photovoltaic energy conversion and photochemical energy storage). 2-5

The atomic-level structures of metal NCs provide ideal systems to probe the correlation between the structure and optical/electronic properties of these ultrasmall nanomaterials.<sup>4–7</sup> While much work has been carried out toward achieving the correlations, many fundamental issues still remain, for instance, the correlation between the structure and carrier dynamics of Au NCs; 4,5 in particular, how does the electronphonon coupling affect the photoexcited carrier lifetime?<sup>8-13</sup> Temperature-dependent optical absorption measurements can provide insights into the fundamental electron-phonon coupling since cryogenic measurements offer a direct way to extract information on electron-phonon coupling and phonon modes.<sup>14</sup> In previous work, this method has been commonly used to characterize conventional semiconductors, perovskite materials, and conjugated organic molecules. 15-18 However, temperature-dependent optical properties of Au NCs are still barely studied.

Ramakrishna et al. reported the first temperature-dependent optical absorption measurements (down to 77 K), which provided deep insights into the electron–phonon coupling and exciton–phonon coupling in Au-thiolate (SR) NCs. <sup>19,20</sup> Their work focused on the comparison of Au NCs of known structures containing  $Au_{13}$  icosahedral ( $I_h$ ) core or fused ones,

i.e., Au<sub>25</sub> sphere vs Au<sub>25</sub> rod.<sup>21–23</sup> In previous solution-based tests (note: "glass" was formed at sufficiently low temperatures), core—shell electron—phonon interactions were identified as the dominant contributor to the optical properties of sphere-like Au<sub>25</sub> and bi-icosahedral Au<sub>38</sub> NCs.<sup>19,20</sup> In contrast, the rod-like Au<sub>25</sub>—which was protected by ternary ligands (SR, PPh<sub>3</sub>, and Cl)<sup>22,23</sup> and possessed no staple motifs—was found to have much weaker electron—phonon coupling strength.<sup>20</sup> Despite these interesting discoveries, no core phonon was identified except the surface staple phonon, which was perplexing and motivated our current work.

Herein, we report the observation of the core phonon of  $Au_{25}$  NCs by a solid thin-film-based method. Specifically, our cryogenic optical absorption spectroscopic measurements are based on polystyrene thin films of the icosahedral  $[Au_{25}(PET)_{18}]^-$  NC (where PET = 2-phenylethanethiolate, simplified as  $I_h$   $Au_{25}$  hereafter owing to its icosahedral core). By adopting the thin-film technique, the testing range of temperature-dependent absorption spectra can be extended down to liquid helium temperature. Lowering the temperature minimizes the peak broadening and can lead to observation of fine features or new trends in the temperature-dependent spectra. By combining the  $Au_{25}$  solution and film-based

Received: January 6, 2021 Accepted: February 1, 2021 Published: February 9, 2021





cryogenic optical measurements, the distinct effect of physical environments on the active phonon modes is discovered, which will open up new opportunities for investigating the electron—phonon coupling and phonon properties of metal NCs.

The synthesis of  $I_h$  Au<sub>25</sub> followed our earlier report.<sup>24</sup> The Au<sub>25</sub> NCs were then embedded in a polystyrene thin film, which was made by a drop-cast method (see details in the Supporting Information). Cryogenic spectroscopic measurements were performed from room temperature down to 15 K. Figure 1 shows the temperature-dependent optical absorption

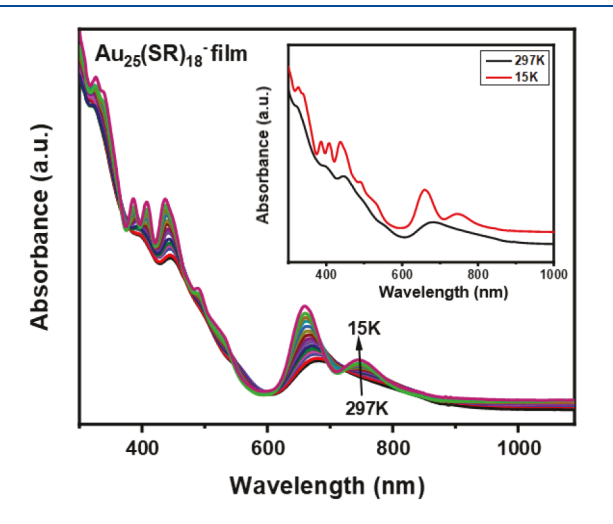


**Figure 1.** Cryogenic optical absorption spectra at different temperatures of  $Au_{25}$  in a thin film of polystyrene. The inset shows the spectra at room temperature and 15 K.

spectra of  $I_h$  Au<sub>25</sub> in a solid film. At room temperature, the spectrum shows three main peaks at 400, 450, and 675 nm (Figure 1 inset, black profile). The observed optical absorption features in the solid sample are consistent with the solution-phase spectrum. When the temperature decreased, several new features appeared in the 300–600 nm region of the spectra of the Au<sub>25</sub> film, and the initially broad peak at 675 nm was also split into two sharp peaks at 660 and 740 nm. Additionally, the absorption spectra of the  $I_h$  Au<sub>25</sub> film exhibited a distinct blueshift of the absorption maxima and an increase in the oscillator strength at low temperatures.

For a comparison between the film- and solution-based systems, we also measured the temperature-dependent absorption spectra of  $I_h$  Au<sub>25</sub> dissolved in 2-methyltetrahydrofuran (a "glass"-forming solvent). Similar optical absorption spectra and temperature-dependent trends were observed (Figure S1), and our results of  $I_h$  Au<sub>25</sub> solution (note: "glass" was formed at sufficiently low temperatures) are similar to the previous observations by Ramakrishna et al. <sup>19</sup> While the spectroscopic trends of the film and solution measurements are qualitatively similar, quantitative analyses reveal some interesting differences in the phonon modes coupled with the electronic transitions (*vide infra*).

Among all the temperature-dependent optical absorption features, the shift of absorption maximum is the most valuable one, because it indicates a change to the corresponding electronic transition gap and such a change discloses information on thermal lattice contraction/expansion and electron—phonon coupling. Ramakrishna et al. 19,20 previously applied a modified Bose—Einstein relationship that was developed by O'Donnell and Chen 17 to model the absorption peak dependence on the temperature and obtained the electron—phonon coupling strength and average phonon

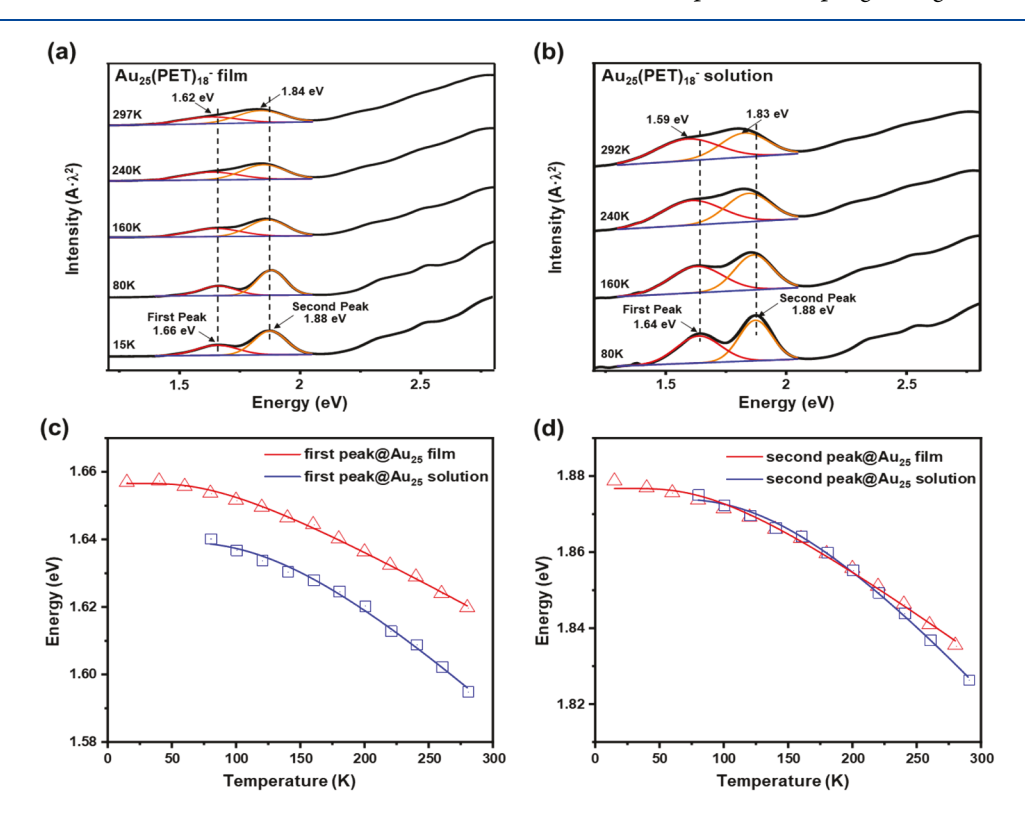


Figure 2. Photon energy-scale spectra and the curve fitting of the 1.3–2.1 eV region at different temperatures for  $I_h$  Au<sub>25</sub> in (a) thin film and (b) solution. Below, the trends and fitting results of absorption maxima with temperature are shown in (c) the first peak and (d) the second peak.

energy for Au NCs in solution. Here, we use the same method to analyze the temperature-dependent energy gap  $(E_{\sigma})$  in our solid film samples. The analytical form of the O'Donnell-Chen equation can be written as

$$E(T) = E(0) - \langle C \rangle \langle \hbar \omega \rangle \left[ \coth \left( \frac{\langle \hbar \omega \rangle}{2kT} \right) - 1 \right]$$
 (1)

where  $\langle \hbar \omega \rangle$  represents the average energy of phonons that contribute to the electron-phonon coupling of the specific electronic transition,  $\langle C \rangle$  is the coupling constant which indicates the electron-phonon coupling strength, and E(0) is the corresponding electronic transition gap at 0 K. We note that the HOMO-LUMO transition energy differs from the value of the HOMO-LUMO gap energy. The latter is typically obtained by extrapolating the optical absorbance to zero, while the HOMO-LUMO transition energy will shift to the blue due to Franck-Condon vertical transition. When we analyze the shift of E(T), an accuracy of  $\sim$ 0.01 eV is required due to the overall small shift, but the method of absorbance extrapolation leads to large errors; thus, we use the peak position, rather than the onset position of absorption, to carry out our data analysis.

In order to better determine the peak position, the wavelength-scale absorption spectra are first transformed to the photon energy (eV)-scale spectra, that is, the plot of absorption intensity  $(A\lambda^2)$ , where A is the absorbance and  $\lambda$  is the wavelength) vs photon energy (Figure 2a,b). Furthermore, we fit the absorption peaks to Gaussian profiles to obtain the accurate positions of absorption maxima. Two Gaussian peaks are needed to reproduce the line shape in the region between 1.3 and 2.1 eV of the  $I_h$  Au<sub>25</sub> (Figure 2a,b). The successful peak deconvolution (Tables S1 and S2) permits us to analyze the two lowest-energy peaks, as opposed to one peak only in Ramakrishna's analysis. 19 Different electronic transitions may couple with different phonon modes. Previous density functional theory (DFT) calculations revealed that the 1.8 eV peak (675 nm) was the HOMO-LUMO transition of Au<sub>25</sub>, but later refinements found a splitting in this region, indicating that the first (1.6 eV) and second (1.8 eV) peaks arise respectively from HOMO-to-LUMO and HOMO-1-to-LUMO transitions.<sup>26</sup>

The first peak (HOMO-to-LUMO transition) of Au<sub>25</sub> in the solid film shows a 0.04 eV blueshift when the temperature decreases from room temperature to 15 K. The positions of this peak are different in the two different environments, solid state vs solution (Figure 2c). At room temperature, the first peak in solution is 0.03 eV lower than that in the solid state, and as the temperature decreases, the difference between the film and solution values becomes slightly smaller. The shape and full width at half-maximum (fwhm, Tables S1 and S2) of peaks for the film and solution samples share a close resemblance, suggesting that the effects of solvation and collisions<sup>27</sup> are less significant in our cases. The second peak of  $I_h$  Au<sub>25</sub> presents a similar temperature-dependent blueshift (Figure 2d). For a quantitative fitting analysis, we employ the O'Donnell-Chen equation to obtain the intrinsic information on  $I_h$  Au<sub>25</sub>. The fitting curves are shown in Figure 2c,d, and the fitting parameters are listed in Table 1.

From Table 1, it can be seen that the average energies of phonons for the first and second absorption peaks of Au<sub>25</sub> are almost the same in either environment (e.g., 23 vs 25 meV in film, 42 vs 43 meV in solution), and so is the coupling

Table 1. Transition Energy at 0 K (E(0)), Average Phonon Energy ( $\langle \hbar \omega \rangle$ ), and Electron-Phonon Coupling Constant  $(\langle C \rangle)$  for Sphere-like  $I_h$  Au<sub>25</sub> in Thin Film and Solution, as Well as Rod-like Au<sub>25</sub> in Thin Film<sup>a</sup>

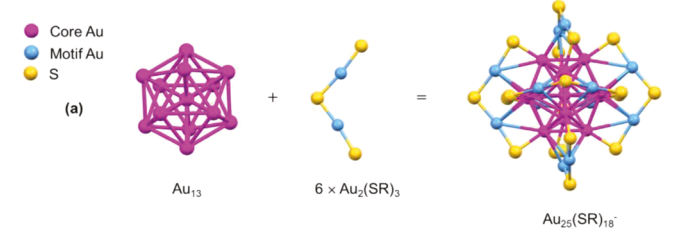
sar	nple	<i>E</i> (0) (eV)	$\langle\hbar\omega angle \ ({ m meV})$	$\langle C \rangle$
[Au <sub>25</sub> (SR) <sub>18</sub> ] <sup>-</sup> solid film	1st peak 2nd peak	$1.661 \pm 0.001$ $1.877 \pm 0.001$	$23 \pm 2$ $25 \pm 2$	$1.3 \pm 0.1$ $1.4 \pm 0.1$
	1st peak 2nd peak	$1.64 \pm 0.001$ $1.874 \pm 0.001$	$42 \pm 4$ $43 \pm 3$	$2.4 \pm 0.2$ $2.5 \pm 0.2$
$ [\mathrm{Au_{25}}(\mathrm{PPh_3})_{10}(\mathrm{SR})_5\mathrm{Cl_2}]^{2+} \text{ solid} $ film		$1.88 \pm 0.01$	18 ± 2	$1.8 \pm 0.1$

<sup>a</sup>See additional data in Figure S2 and Table S3. All parameters are obtained by fitting the data of the temperature-dependent absorption spectra.

constant. These results suggest that the electronic transitions from the doubly degenerate 1P<sub>3/2</sub> to LUMO and nondegenerate  $1P_{1/2}$  to LUMO couple with the same phonon mode. Interestingly, when comparing the two different environments, we found that the average phonon energy for the case of Au<sub>25</sub> film is significantly smaller than that of Au<sub>25</sub> in solution (24 vs 42.5 meV), and so is the coupling constant (1.35 vs 2.45). These differences indicate that the solutionstate Au<sub>25</sub> phonons and electron-phonon coupling strength are suppressed in the solid state, leading to the manifestation or exposure of new phonons and their coupling with the electronic transitions in the Au<sub>25</sub> solid state. Below we rationalize the phonon modes that couple with the first and second peaks of Au<sub>25</sub> in solution and solid states.

Unlike small molecules, [Au<sub>25</sub>(SCH<sub>2</sub>CH<sub>2</sub>Ph)<sub>18</sub>] possesses 349 atoms, and its number of vibrational normal modes is very large (i.e., 3N-6 = 1041, where N = 349 atoms); all these modes form a quite dense distribution that can be represented by the vibrational density of states. 28-32 The assignment of vibrational (phonon) modes relies on the structure-based DFT calculations on Au<sub>25</sub>(SR)<sub>18</sub> NCs<sup>28-32</sup> and experimental results from far-infrared absorption and terahertz Raman scattering measurements of Au NCs. 33-38 The structure of the  $I_h$  Au<sub>25</sub> possesses an icosahedral Au<sub>13</sub> core and six Au<sub>2</sub>(SR)<sub>3</sub> dimeric surface motifs (Scheme 1). DFT calculations of the Au<sub>25</sub>

Scheme 1. Core-Shell Structure of Au<sub>25</sub>(SR)<sub>18</sub>



<sup>a</sup>Redrawn from ref 21.

vibrational properties by Tlahuice-Flores et al. revealed that the 0-350 cm<sup>-1</sup> region hosts the Au-S-Au bending modes, the core breathing and staple breathing modes, and the Au–S stretching modes. <sup>29,30</sup> The core modes (including the breathing mode and Au-Au stretching ones) are in the range of  $0-120~{\rm cm}^{-1}$  for  ${\rm Au}_{25}({\rm SR})_{18}$  with R = CH<sub>3</sub> or CH<sub>2</sub>CH<sub>3</sub>,  $^{28-30}$  but with increasing the R group size to

Table 2. Theoretical Vibrational (Phonon) Modes of Au<sub>25</sub>(SR)<sub>18</sub> Nanoclusters<sup>a</sup>

DFT model	core (cm <sup>-1</sup> )	core-shell Au <sub>core</sub> -S (cm <sup>-1</sup> )	shell Au <sup>I</sup> –S (cm <sup>-1</sup> )	refs		
$[Au_{25}(SCH_3)_{18}]^-$	103.8 (core breathing)	240 (stretching)	268.6 (staple breathing), 174.4 (S-CH $_3$ bending)	29, 30		
$[Au_{25}(SC_2H_5)_{18}]^-$	20-120 (various modes of the core)		$320/375 \; (Au^I - S \; stretching)$	36		
$[{ m Au}_{25}({ m PET})_{18}]^-$	110 (core breathing) 150–180 (stretching)	325 (stretching)	303 (breathing), 360 (stretching), 205/230 (bending)	31		
<sup>a</sup> Note: Au _ = the core gold stom Au <sup>I</sup> = the stanle gold stom and DET = SCH CH Dh						

<sup>a</sup>Note: Au<sub>core</sub> = the core gold atom, Au<sup>I</sup> = the staple gold atom, and PET = SCH<sub>2</sub>CH<sub>2</sub>Ph.

 ${
m CH_2CH_2Ph}$ , Häkkinen and co-workers<sup>31</sup> found that the core modes span a wider range (0 to 180 cm<sup>-1</sup>), with the 150–180 cm<sup>-1</sup> region mainly consisting of Au–Au stretching modes of the Au<sub>13</sub> core. Table 2 compiles these literature results, which together with other reports<sup>32–38</sup> facilitates our assignment of phonons in electron–phonon coupling of Au<sub>25</sub> below. Note that the modes with frequencies of 400–4000 cm<sup>-1</sup> are solely from the organic tail (R group)<sup>30</sup> and are not listed in Table 2.

Bürgi and co-workers 36,37 performed detailed investigations on the staple Au<sup>I</sup>-S vibrations and found a range of 250-360 cm<sup>-1</sup>. These modes are consistent with theory 28-31,36 (Table 2). In our cryogenic optical measurements, the observed ~350 cm<sup>-1</sup> (42-43 meV) phonon mode that couples with the first and second absorption peaks of Au<sub>25</sub> in solution is assigned to the staple Au<sup>I</sup>-S stretching of the Au<sub>2</sub>(SR)<sub>3</sub> motif. <sup>19,33,37</sup> In contrast, the phonon mode for the Au<sub>25</sub> film case is much lower than that for the Au<sub>25</sub> solution case, indicating that the corresponding electronic transitions no longer couple with the surface-motif phonon mode in the solid state. We attribute the absence of the  ${\sim}350~\text{cm}^{-1}$  phonon mode in the  $\text{Au}_{25}$  film to the suppression of Au-S-Au-S-Au vibrations by intracluster and cluster-matrix interactions in the solid state.<sup>39</sup> Specifically, the benzene rings from PET ligands can form intracluster C- $H \cdots \pi$  interactions (Figure S3), which suppress the free vibrations of the staple motifs. In addition, the stronger Coulomb interaction between [Au<sub>25</sub>(PET)<sub>18</sub>]<sup>-</sup> and its counterion <sup>+</sup>N(C<sub>8</sub>H<sub>17</sub>)<sub>4</sub> owing to the bound state in solids can also restrain the vibrations of staple motifs. Based upon the previous calculations on  $[Au_{25}(PET)_{18}]^-$  (Table 2), we assign the observed  $\sim 180$  cm<sup>-1</sup> (22–23 meV) phonon to the core mode (Au-Au stretching<sup>31</sup>). This average phonon energy should correspond to the optical phonons of the Au<sub>13</sub> core, as opposed to the lower-frequency acoustic phonons (both the breathing and quadrupolar deformation modes) of the core. The breathing mode involves the totally symmetric, radial expansion/contraction and is typically below ~120 cm<sup>-1</sup> for different-sized Au<sub>n</sub>(SR)<sub>m</sub> NCs. 30,40 Both the breathing mode and the quadrupolar deformation mode<sup>30</sup> are often observed in ultrafast electron dynamics. 4,11,12,32,41,42

We also note that the  $180~\rm cm^{-1}$  core phonon for the sphere-like  $I_h$   $Au_{25}$  in the film state is comparable to the  $150~\rm cm^{-1}$  (18 meV) phonon mode observed in the rod-like  $Au_{25}$  (see data in Figure S2 and Table S3), which consists of two icosahedral  $Au_{13}$  units sharing a common vertex Au atom (Figure S4). Since there is no staple motif in the rod-like  $Au_{25}$  structure, the phonon mode of  $150~\rm cm^{-1}$  (18 meV) should arise from the core vibrations in the  $Au_{13}$  dimer. DFT simulations by Akola and co-workers reported vibrational modes of  $107~\rm and$   $144~\rm cm^{-1}$  for the rod-like  $Au_{25}$ . We note that our result of the rod-like  $Au_{25}$  (core phonon:  $150~\rm cm^{-1}$ ) is very close to the ealier

reported solution result  $(160 \text{ cm}^{-1})$ .<sup>2</sup> Thus, the results on rod-like Au<sub>25</sub>—which possesses a bi-icosahedral core but no staple motifs—also support the assignment for the sphere-like  $I_h$  Au<sub>25</sub>. The observed ~180 cm<sup>-1</sup> phonon mode of the sphere-like  $I_h$  Au<sub>25</sub> in films should arise from the Au core vibrations and is optically active.

In summary, we have investigated the temperature-dependent optical absorption of [Au<sub>25</sub>(PET)<sub>18</sub>]<sup>-</sup> in both solution and solid-state environments. The film-based method extends the temperature to the liquid helium temperatures. The temperature-dependent absorption data analyses through peak deconvolution and fitting with a theoretical model make it possible to extract the Au-S shell phonon mode and the Au core phonon mode in  $I_h$  Au<sub>25</sub>. The first two absorption peaks (lowest-energy) for the  $I_h$  Au<sub>25</sub> in solution are found to couple with the shell phonon mode (~350 cm<sup>-1</sup>) with strong coupling strength, but the solid state gives rise to the coupling with the core phonon mode (~180 cm<sup>-1</sup>) with weak coupling strength. The suppression of shell phonon modes in the  $I_h$  Au<sub>25</sub> solid state is ascribed to intracluster and cluster-matrix interactions. Our findings demonstrate the temperaturedependent optical spectroscopic analysis for gaining important information about electron-phonon coupling and the associated phonon modes. Future work will lead to more fundamental understanding of phonon-coupled optical properties<sup>5,7,44,45</sup> and electron dynamics, <sup>8,32,41,42</sup> as well as the evolution of phonon properties with size<sup>30,41,46</sup> for metal nanoclusters, and based upon such progress, new applications of atomically precise nanoclusters will be developed.

## ASSOCIATED CONTENT

# **Supporting Information**

The Supporting Information is available free of charge at https://pubs.acs.org/doi/10.1021/acs.jpclett.1c00050.

Experimental section; absorption spectra of  $Au_{25}$  solution (Figure S1); absorption spectra of rod-like  $Au_{25}$  film (Figure S2); intracluster interaction of  $Au_{25}$  sphere (Figure S3); structure of  $Au_{25}$  rod (Figure S4); and data for deconvoluted peaks (Tables S1–S3) (PDF)

## AUTHOR INFORMATION

## **Corresponding Author**

Rongchao Jin — Department of Chemistry, Carnegie Mellon University, Pittsburgh, Pennsylvania 15213, United States; orcid.org/0000-0002-2525-8345; Email: rongchao@andrew.cmu.edu

#### **Authors**

- Zhongyu Liu Department of Chemistry, Carnegie Mellon University, Pittsburgh, Pennsylvania 15213, United States; orcid.org/0000-0002-2777-8360
- Yingwei Li Department of Chemistry, Carnegie Mellon University, Pittsburgh, Pennsylvania 15213, United States; orcid.org/0000-0002-4813-6009
- Wonyong Shin Department of Chemistry, Carnegie Mellon University, Pittsburgh, Pennsylvania 15213, United States

Complete contact information is available at: https://pubs.acs.org/10.1021/acs.jpclett.1c00050

#### **Notes**

The authors declare no competing financial interest.

## ACKNOWLEDGMENTS

R.J. acknowledges financial support from the National Science Foundation (NSF) under Grant No. DMR-1808675.

## REFERENCES

- (1) Jin, R.; Li, G.; Sharma, S.; Li, Y.; Du, X. Toward Active-Site Tailoring in Heterogeneous Catalysis by Atomically Precise Metal Nanoclusters with Crystallographic Structures. *Chem. Rev.* **2021**, *121*, 567–648
- (2) Chen, Y.-S.; Choi, H.; Kamat, P. V. Metal-Cluster-Sensitized Solar Cells. A New Class of Thiolated Gold Sensitizers Delivering Efficiency Greater Than 2%. *J. Am. Chem. Soc.* **2013**, *135*, 8822–8825.
- (3) Abbas, M. A.; Kamat, P. V.; Bang, J. H. Thiolated Gold Nanoclusters for Light Energy Conversion. *ACS Energy Lett.* **2018**, 3, 840–854.
- (4) Zhou, M.; Jin, R. Optical Properties and Excited-State Dynamics of Atomically Precise Gold Nanoclusters. *Annu. Rev. Phys. Chem.* 2021, 72, 72
- (5) Weerawardene, K. D. M.; Pandeya, P.; Zhou, M.; Chen, Y.; Jin, R.; Aikens, C. M. Luminescence and Electron Dynamics in Atomically Precise Nanoclusters with Eight Superatomic Electrons. *J. Am. Chem. Soc.* **2019**, *141*, 18715–18726.
- (6) Jin, R.; Zeng, C.; Zhou, M.; Chen, Y. Atomically Precise Colloidal Metal Nanoclusters and Nanoparticles: Fundamentals and Opportunities. *Chem. Rev.* **2016**, *116*, 10346–10413.
- (7) Kang, X.; Zhu, M. Tailoring the Photoluminescence of Atomically Precise Nanoclusters. *Chem. Soc. Rev.* **2019**, *48*, 2422–2457
- (8) Zhou, M.; Higaki, T.; Hu, G.; Sfeir, M. Y.; Chen, Y.; Jiang, D.-E.; Jin, R. Three-Orders-of-Magnitude Variation of Carrier Lifetimes with Crystal Phase of Gold Nanoclusters. *Science* **2019**, *364*, 279–282.
- (9) Zhou, M.; Higaki, T.; Li, Y.; Zeng, C.; Li, Q.; Sfeir, M. Y.; Jin, R. Three-Stage Evolution from Nonscalable to Scalable Optical Properties of Thiolate-Protected Gold Nanoclusters. *J. Am. Chem. Soc.* **2019**, *141*, 19754–19764.
- (10) Zhou, M.; Jin, R.; Sfeir, M. Y.; Chen, Y.; Song, Y.; Jin, R. Electron Localization in Rod-Shaped Triicosahedral Gold Nanocluster. *Proc. Natl. Acad. Sci. U. S. A.* **2017**, *114*, E4697—E4705.
- (11) Kwak, K.; Thanthirige, V. D.; Pyo, K.; Lee, D.; Ramakrishna, G. Energy Gap Law for Exciton Dynamics in Gold Cluster Molecules. *J. Phys. Chem. Lett.* **2017**, *8*, 4898–4905.
- (12) Varnavski, O.; Ramakrishna, G.; Kim, J.; Lee, D.; Goodson, T. Critical Size for the Observation of Quantum Confinement in Optically Excited Gold Clusters. *J. Am. Chem. Soc.* **2010**, *132*, 16–17.
- (13) Higaki, T.; Zhou, M.; He, G.; House, S. D.; Sfeir, M. Y.; Yang, J. C.; Jin, R. Anomalous Phonon Relaxation in Au<sub>333</sub>(SR)<sub>79</sub> Nanoparticles with Nascent Plasmons. *Proc. Natl. Acad. Sci. U. S. A.* **2019**, *116*, 13215–13220.
- (14) Huang, K.; Rhys, A. Theory of Light Absorption and Non-radiative Transitions in F-centres. *Proc. R. Soc. London A* **1950**, 204, 406–423.

- (15) Hoch, F. L. Low-Temperature Absorption Spectroscopy (Cryoabsorption Spectroscopy). J. Chem. Educ. 1955, 32, 469.
- (16) Varshni, Y. P. Temperature Dependence of the Energy Gap in Semiconductors. *Physica* **1967**, *34*, 149–154.
- (17) O'Donnell, K.; Chen, X. Temperature Dependence of Semiconductor Band Gaps. Appl. Phys. Lett. 1991, 58, 2924–2926.
- (18) Kok, D. J.; Irmscher, K.; Naumann, M.; Guguschev, C.; Galazka, Z.; Uecker, R. Temperature-Dependent Optical Absorption of SrTiO<sub>3</sub>. *Phys. Status Solidi A* **2015**, *212*, 1880–1887.
- (19) Devadas, M. S.; Bairu, S.; Qian, H.; Sinn, E.; Jin, R.; Ramakrishna, G. Temperature-Dependent Optical Absorption Properties of Monolayer-Protected Au<sub>25</sub> and Au<sub>38</sub> Clusters. *J. Phys. Chem. Lett.* **2011**, *2*, 2752–2758.
- (20) Devadas, M. S.; Thanthirige, V. D.; Bairu, S.; Sinn, E.; Ramakrishna, G. Temperature-Dependent Absorption and Ultrafast Luminescence Dynamics of Bi-icosahedral Au<sub>25</sub> Clusters. *J. Phys. Chem. C* **2013**, *117*, 23155–23161.
- (21) Zhu, M.; Aikens, C. M.; Hollander, F. J.; Schatz, G. C.; Jin, R. Correlating the Crystal Structure of a Thiol-Protected Au<sub>25</sub> Cluster and Optical Properties. *J. Am. Chem. Soc.* **2008**, *130*, 5883–5885.
- (22) Shichibu, Y.; Negishi, Y.; Watanabe, Ta; Chaki, N. K.; Kawaguchi, H.; Tsukuda, T. Biicosahedral Gold Clusters  $[\mathrm{Au}_{25}(\mathrm{PPh}_3)_{10}(\mathrm{SC}_n\mathrm{H}_{2n+1})_5\mathrm{Cl}_2]^{2+}$  (n=2-18): A Stepping Stone to Cluster-Assembled Materials. J. Phys. Chem. C **2007**, 111, 7845–7847.
- (23) Qian, H.; Eckenhoff, W. T.; Bier, M. E.; Pintauer, T.; Jin, R. Crystal Structures of Au<sub>2</sub> Complex and Au<sub>25</sub> Nanocluster and Mechanistic Insight into the Conversion of Polydisperse Nanoparticles into Monodisperse Au<sub>25</sub> Nanoclusters. *Inorg. Chem.* **2011**, *50*, 10735–10739.
- (24) Zhu, M.; Lanni, E.; Garg, N.; Bier, M. E.; Jin, R. Kinetically Controlled, High-yield Synthesis of Au<sub>25</sub> Clusters. *J. Am. Chem. Soc.* **2008**, *130*, 1138–1139.
- (25) Murray, R. W. Nanoelectrochemistry: Metal Nanoparticles, Nanoelectrodes, and Nanopores. *Chem. Rev.* **2008**, *108*, 2688–2720. (26) Jiang, D.-E.; Kühn, M.; Tang, Q.; Weigend, F. Superatomic Orbitals under Spin-Orbit Coupling. *J. Phys. Chem. Lett.* **2014**, *5*, 3286–3289.
- (27) Bulović, V.; Burrows, P.; Forrest, S.; Cronin, J.; Thompson, M. Study of Localized and Extended Excitons in 3, 4, 9, 10-Perylenetetracarboxylic Dianhydride (PTCDA) I. Spectroscopic Properties of Thin Films and Solutions. *Chem. Phys.* **1996**, 210, 1–12.
- (28) Guberman-Pfeffer, M. J.; Ulcickas, J.; Gascón, J. A. Connectivity-Based Biocompatible Force Field for Thiolated Gold Nanoclusters. *J. Phys. Chem. C* **2015**, *119*, 27804–27812.
- (29) Tlahuice-Flores, A. Normal Modes of  $Au_{25}(SCH_3)_{18}^-$ ,  $Ag_{12}Au_{13}(SCH_3)_{18}^-$ , and  $Ag_{25}(SCH_3)_{18}^-$  Clusters. *Mol. Simul.* **2013**, 39, 428–431.
- (30) Tlahuice-Flores, A.; Whetten, R. L.; Jose-Yacaman, M. Vibrational Normal Modes of Small Thiolate-Protected Gold Clusters. *J. Phys. Chem. C* **2013**, *117*, 12191–12198.
- (31) Akola, J.; Kacprzak, K. A.; Lopez-Acevedo, O.; Walter, M.; Grönbeck, H.; Häkkinen, H. Thiolate-Protected Au<sub>25</sub> Superatoms as Building Blocks: Dimers and Crystals. *J. Phys. Chem. C* **2010**, *114*, 15986–15994.
- (32) Senanayake, R. D.; Akimov, A. V.; Aikens, C. M. Theoretical Investigation of Electron and Nuclear Dynamics in the  $[Au_{25}(SH)_{18}]^{-1}$  Thiolate-Protected Gold Nanocluster. *J. Phys. Chem.* C 2017, 121, 10653–10662.
- (33) Petroski, J.; Chou, M.; Creutz, C. The Coordination Chemistry of Gold Surfaces: Formation and Far-Infrared Spectra of Alkanethiolate-Capped Gold Nanoparticles. *J. Organomet. Chem.* **2009**, *694*, 1138–1143.
- (34) Parker, J. F.; Choi, J. P.; Wang, W.; Murray, R. W. Electron Self-Exchange Dynamics of the Nanoparticle Couple [Au<sub>25</sub>(SC<sub>2</sub>Ph)<sub>18</sub>]<sup>0/1-</sup> By Nuclear Magnetic Resonance Line-Broadening. *J. Phys. Chem. C* **2008**, *112*, 13976–13981.
- (35) Antonello, S.; Arrigoni, G.; Dainese, T.; De Nardi, M.; Parisio, G.; Perotti, L.; René, A.; Venzo, A.; Maran, F. Electron Transfer

- Through 3D Monolayers on  $Au_{25}$  Clusters. ACS Nano 2014, 8, 2788–2795.
- (36) Varnholt, B.; Oulevey, P.; Luber, S.; Kumara, C.; Dass, A.; Bürgi, T. Structural Information on the Au-S Interface of Thiolate-Protected Gold Clusters: A Raman Spectroscopy Study. *J. Phys. Chem.* C **2014**, *118*, 9604–9611.
- (37) Bürgi, T. Properties of the Gold-Sulphur Interface: from Self-Assembled Monolayers to Clusters. *Nanoscale* **2015**, *7*, 15553–15567.
- (38) Kato, M.; Shichibu, Y.; Ogura, K.; Iwasaki, M.; Sugiuchi, M.; Konishi, K.; Yagi, I. Terahertz Raman Spectroscopy of Ligand-Protected Au. Clusters. *J. Phys. Chem. Lett.* **2020**, *11*, 7996–8001.
- (39) Li, Y.; Jin, R. Seeing Ligands on Nanoclusters and in Their Assemblies by X-ray Crystallography: Atomically Precise Nanochemistry and Beyond. *J. Am. Chem. Soc.* **2020**, *142*, 13627–13644.
- (40) Palacios-Álvarez, O.; Tlahuice-Flores, A. Tri-icosahedral Au<sub>37</sub> Cluster as a Carrier/Detector for Anti-Cancer Cisplatin Drug. *J. Raman Spectrosc.* **2019**, *50*, 52–62.
- (41) Maioli, P.; Stoll, T.; Sauceda, H. E.; Valencia, I.; Demessence, A.; Bertorelle, F.; Crut, A.; Vallee, F.; Garzon, I. L.; Cerullo, G.; Del Fatti, N. Mechanical Vibrations of Atomically Defined Metal Clusters: From Nano-to Molecular-Size Oscillators. *Nano Lett.* **2018**, *18*, 6842–6849.
- (42) Williams, L. J.; Herbert, P. J.; Tofanelli, M. A.; Ackerson, C. J.; Knappenberger, K. L., Jr Superatom Spin-State Dynamics of Structurally Precise Metal Monolayer-Protected Clusters (MPCs). J. Chem. Phys. 2019, 150, 101102.
- (43) Goh, J.-Q.; Malola, S.; Häkkinen, H.; Akola, J. Role of the Central Gold Atom in Ligand-Protected Biicosahedral Au<sub>24</sub> and Au<sub>25</sub> Clusters. *J. Phys. Chem. C* **2013**, *117*, 22079–22086.
- (44) Green, T. D.; Yi, C.; Zeng, C.; Jin, R.; McGill, S.; Knappenberger, K. L., Jr Temperature-Dependent Photoluminescence of Structurally-Precise Quantum-Confined Au<sub>25</sub>(SC<sub>8</sub>H<sub>9</sub>)<sub>18</sub> and Au<sub>38</sub>(SC<sub>12</sub>H<sub>25</sub>)<sub>24</sub> Metal Nanoparticles. *J. Phys. Chem. A* **2014**, *118*, 10611–10621.
- (45) Toh, Y.-R.; Yu, P.; Wen, X.; Tang, J. The Enhancement of Electron-Phonon Coupling in Glutathione-Protected Au<sub>25</sub> Clusters. *J. Colloid Interface Sci.* **2013**, 402, 86–89.
- (46) Sauceda, H. E.; Garzón, I. L. Structural Determination of Metal Nanoparticles from Their Vibrational (Phonon) Density of States. *J. Phys. Chem. C* **2015**, *119*, 10876–10880.